EEG Quality: The Image Acquisition Artefact

9

Petra Ritter, Robert Becker, Frank Freyer, and Arno Villringer

Abbreviations

ANC	Adaptive noise cancellation
FASTR	FMRI artefact slice template removal
FT	Fourier transform
IAR	Imaging artefact reduction
ICA	Independent component analysis
ITAS	Interpolation–template–alignment–subtraction
LPF	Low-pass filter
PCA	Principal component analysis
RF	Radiofrequency
SNR	Signal-to-noise ratio
TDC	Template drift compensation
TDD	Template drift detection

1 Origin of the Image Acquisition Artefact

In this chapter, we focus on the artefacts that arise in the EEG during the fMRI acquisition process. Functional MRI using echo planar imaging (EPI) sequences involves the application of rapidly varying magnetic field gradients for spatial encoding of the MR signal and radiofrequency (RF) pulses for spin excitation (see the chapter "The Basics of Functional Magnetic Resonance Imaging"). Early in the implementation of EEG–fMRI, it was observed that the acquisition of an MR image results in complete obscuration of

P. Ritter (✉)
Department of Neurology, Charité Universitätsmedizin Berlin, Charitéplatz 1, 10117 Berlin, Germany
e-mail: Petra.ritter@charite.de

C. Mulert and L. Lemieux (eds.), *EEG– fMRI*

DOI: 10.1007/978-3-540-87919-0_9,

the physiological EEG (Ives et al. 1993; Allen et al. 2000). Electromagnetic induction in the circuit formed by the electrodes, leads, patient and amplifier exposed to a time-varying magnetic field causes an electromotive force. Artefacts induced in the EEG by the scanning process have a strong deterministic component, due to the preprogrammed nature of the RF and gradient switching sequence, and therefore artefact correction is generally considered a lesser problem than pulse-related artefacts (see the chapter "EEG Quality: Origin and Reduction of the EEG Cardiac-Related Artefact"). According to Faraday's law of induction, the induced electromotive force is proportional to the time derivative of the magnetic flux (summation of the magnetic field perpendicular to the circuit plane over the area circuit), $d\Phi/dt$, and can therefore reflect changes in the field (gradient switching, RF) or in the circuit geometry or position relative to the field due to body motion (Lemieux et al. 1997). Therefore, the combination of body motion with image acquisition artefacts can lead to random variations that represent a real challenge for artefact correction.

2 Characteristics of the Image Acquisition Artefact

In a typical EPI BOLD acquisition, the amplitude of the image acquisition artefact can be more than two orders of magnitude higher than the physiological EEG signal (Allen et al. 2000; Felblinger et al. 1999). The largest rate of change of the magnetic field occurs during the application of the RF pulses (about 30,000 T/s) (Huang-Hellinger et al. 1995). However, the frequency of the RF pulses (e.g. 64 MHz at 1.5T), lies well outside the frequency range of conventional EEG amplifiers resulting in greatly attenuated artefacts (Anami et al. 2003). For example, fMRI in a 1.5 T Siemens Magnetom Vision Scanner (Siemens Erlangen, Germany) produced image acquisition artefacts with amplitudes of up to 12 mV (Figs. 1 and 2). At 1.5 and 3 T, artefacts induced by gradient switching (10^3–10^4 μV) are generally much larger than those arising from RF pulses (up to 10^2 μV) (Anami et al. 2003).

The recorded artefact from one gradient pulse has the approximate differential waveform of the corresponding gradient pulse (Anami et al. 2003). The relative polarity and amplitude of the artefact varies across channels, but the timing of the rising and falling edges is the same across all channels. The frequency range of the image acquisition artefact exceeds that of standard clinical EEG equipment. The frequency of the readout gradient typically lies in the range of 500–900 Hz. Figures 1 and 2 illustrate typical time courses of the slice acquisition artefact. During periodic EPI BOLD scanning, the EEG is dominated by harmonics of the slice repetition frequency, typically in the range of 10–25 Hz (Fig. 3), convolved with harmonics of the volume repetition frequency of about 0.2–2 Hz (Mandelkow et al. 2006; Ritter et al. 2008a). The power spectrum of the image acquisition artefact thus overlaps that of the EEG.

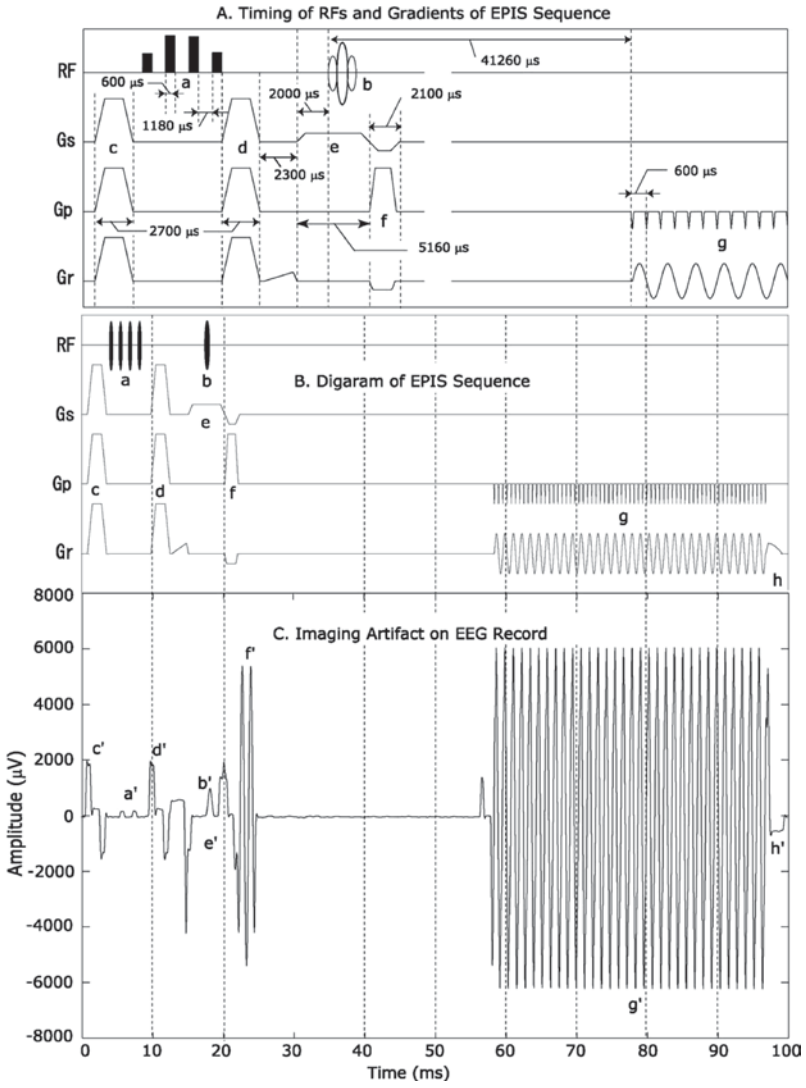

Fig. 1A–C The waveform of the image acquisition artefact can be accurately measured using a sufficiently high digitisation rate and a band-pass filter—here 20kHz/3kHz. This is a representative artefact waveform from a EPI BOLD fMRI (EPI) sequence. **A** Timings of RF and gradients in an fMRI sequence (EPIS, Siemens: ep2d_fid_60b2080_62_64.ekc). *RF*, radiofrequency wave; *Gs*, slice selection gradient; *Gp*, phase encoding gradient; *Gr*, readout gradient. *a*, Fat suppression pulses (1-3-3-1 pulses); *b*, slice selection RF; *c*, *d*, *h*, spoilers; *e*, slice selection gradient; *f*, dephasing and rephasing gradient; *g*, readout gradient. **B** Schematic diagram of whole EPIS sequence. **C** Image acquisition artefact waveform for one slice scan on a dummy EEG record with a phantom using the EPIS sequence. The artefact corresponding to each gradient component described above in **A** can be identified and is denoted by the same alphabet as that denoting the original gradient but with a prime (Anami et al. 2003)

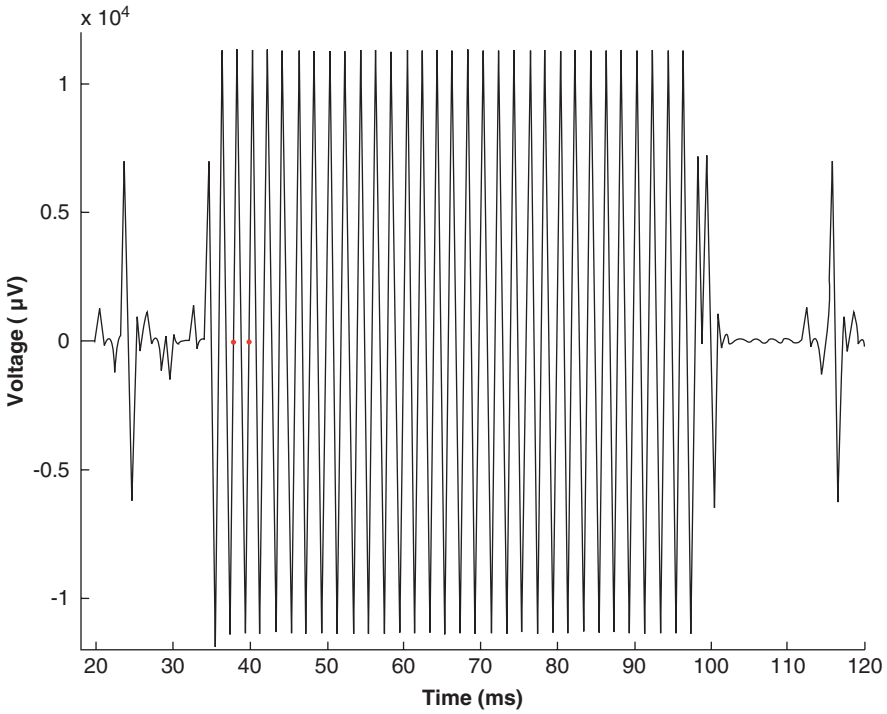

Fig. 2 The waveform of an image acquisition artefact during a single-slice acquisition (stepping stone sequence) using a 1.5 T scanner (Siemens Vision). The artefact was recorded at a sampling rate of 5 kHz and using a 1 kHz hardware low-pass filter. Here the readout gradient has a frequency of 500 Hz (the *two red dots* indicate one gradient period of length 2 ms).

3 Avoiding Image Acquisition Artefacts: Interleaved EEG–fMRI Protocols

Depending on the type of brain activity one is interested in studying, interruptions in scanning can reduce the impact of image acquisition artefacts. In EEG-triggered fMRI, short series of fMRI images are acquired following the (random) occurrence of predefined EEG events such as epileptic discharges (Baudewig et al. 2001; Krakow et al. 1999; Lemieux et al. 2001; Seeck et al. 1998; Symms et al. 1999; Warach et al. 1996). Assuming that the peak of the BOLD changes associated with the neural activity of interest occurs with the same time delay as those of normal stimuli (typically 3–8 s), the delayed onset of fMRI acquisition relative to the neural response does not pose a problem. However, this approach requires that the T1 saturation effects are modelled explicitly (Krakow et al. 2002), and fMRI signal changes that occur over long time scales cannot be easily accounted for, given the irregular sampling.

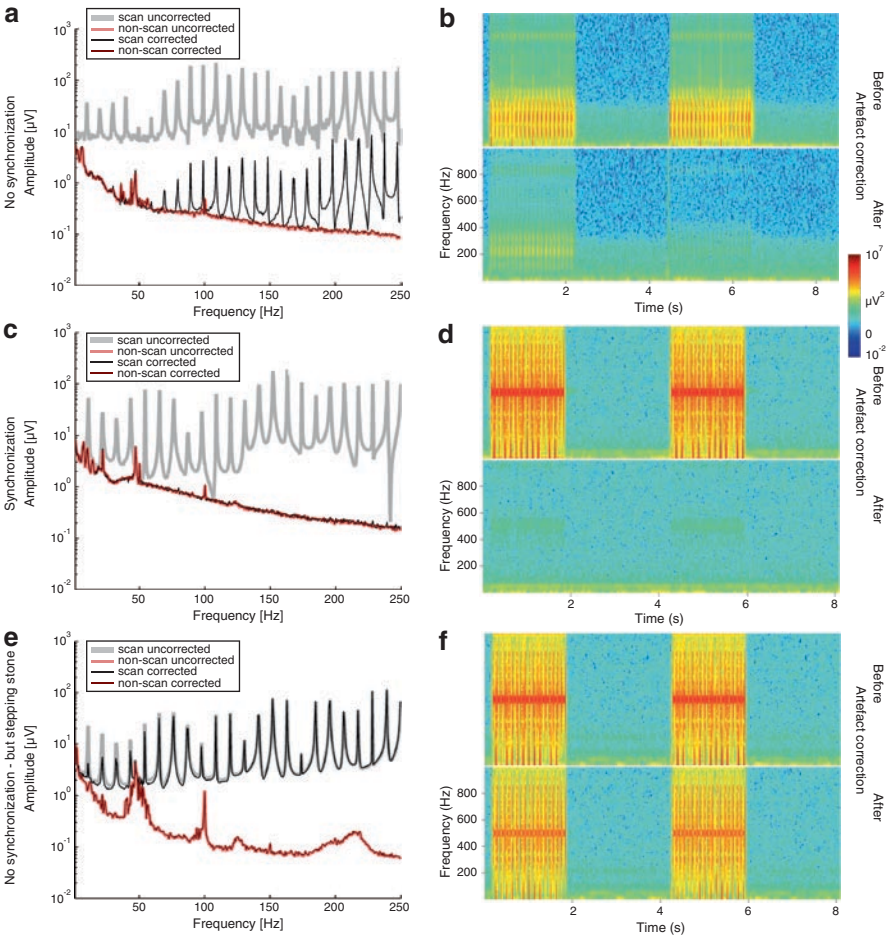

Fig. 3a–f Fourier spectrum and time–frequency plots of EEG data from synchronised and unsynchronised EEG and fMRI data acquisitions before and after image acquisition artefact correction using a slightly modified interpolation–template–alignment–subtraction (ITAS) algorithm (Ritter et al. 2007). Fourier spectra were calculated for scan periods and for non-scan periods. The Fourier spectrum of the imaging artefact afflicted EEG is dominated by harmonics of the slice repetition frequency (10 Hz in this study). **a** Unsynchronised EEG–fMRI (1.5 T Siemens Sonata) with an unstable MR sequence. The application of a correction algorithm comprising interpolation, timing error correction and artefact template subtraction (using a slightly modified ITAS algorithm as described in Ritter et al. 2007) yields good results in the frequency spectrum below 70 Hz. In **b**, for the same EEG data, time–frequency plots *before* and *after* image artefact correction are depicted. **c** Synchronised EEG–fMRI (1.5 T Siemens Vision) with a temporally stable *stepping-stone* MR sequence; simple artefact template subtraction can yield good results across the entire frequency spectrum. **d** Here the time-frequency plot of the imaging artefact corrected EEG data shows only mild residual artefacts in the 500 Hz range, reflecting the switching rate of the readout gradient. **e** Interestingly, the same algorithm used in **a** and **b** is much less efficient when applied to an EEG obtained from an unsynchronised EEG–fMRI setup with a stepping-stone sequence. Strong image acquisition artefacts are visible after imaging artefact correction, even in the lower frequency bands. This failure of the algorithm can be attributed to the oscillatory amplitude fluctuations of the image acquisition artefacts seen in Fig. 4a. **f** Here, the time–frequency plot of the imaging artefact corrected EEG is severely contaminated with residual artefacts.

In the periodic interleaved approach, MR acquisition is suspended at regular intervals, resulting in periods free of image acquisition artefacts on the EEG (Goldman et al. 2000, 2002; Ives et al. 1993; Kruggel et al. 2000; Sommer et al. 2003; Ritter et al. 2008a). Although interleaved protocols are generally less flexible and experimentally efficient than continuous measurements, they are suitable for certain forms of brain activity such as slowly varying rhythms and evoked responses. With longer acquisition times, unintentional fluctuations in attention and vigilance gain more relevance.

In multimodal studies of average evoked potentials/BOLD responses, a simultaneous EEG–fMRI setup is not always necessary (Horovitz et al. 2002, 2004; Opitz et al. 1999). In such cases separate EEG and fMRI measurements offer a reasonable alternative. There are, however, a number of questions that can only be addressed by truly simultaneous EEG–fMRI acquisition, such as studies on single trials and spontaneous non-task-related activity; see the chapters "Principles of Multimodal Functional Imaging and Data Integration" and "Experimental Design and Data Analysis Strategies".

4 Reduction of Image Acquisition Artefacts

4.1 Reduction at the Source

Minimising conductor loop area and avoiding conductor motion should help to reduce image acquisition artefacts in concurrent EEG–fMRI. Movement can be reduced by stabilising the subject's or patient's head with a vacuum cushion and fixing the EEG electronic devices and wires using sandbags, for example (Anami et al. 2003; Benar et al. 2003). Electrodes should be made of nonferromagnetic materials such as silver, silver/silver chloride, gold-coated silver and carbon (Van Audekerkea et al. 2000) in order to prevent motion relative to the scalp resulting from the strong static magnetic field. Artefact-reducing materials for the leads connecting electrode rings and amplifier are, for example, carbon fibres (Goldman et al. 2000) or very thin copper leads (Easy Cap, FMS, Munich). Twisted dual leads have the advantage that currents induced by motion and gradient switching cancel out since the currents induced in consecutive twists flow in opposing directions (Goldman et al. 2000). When possible, switching off the scanner's helium pump and patient monitoring devices can help to reduce vibration- and RF-related artefacts in the EEG (Fig. 4).

4.1.1 Stepping-Stone Sampling

Due to the short durations of image acquisition artefacts, a special MR sequence has been developed that allows EEG sampling at a digitisation rate of 1 kHz exclusively in the period in which the artefact resides around baseline level (Anami et al. 2003). This "stepping stone" sampling of EEG data is only possible in combination with synchronisation of the EEG digitisation and scanner clock. Artefact amplitude is strongly attenuated (Fig. 5d), for example

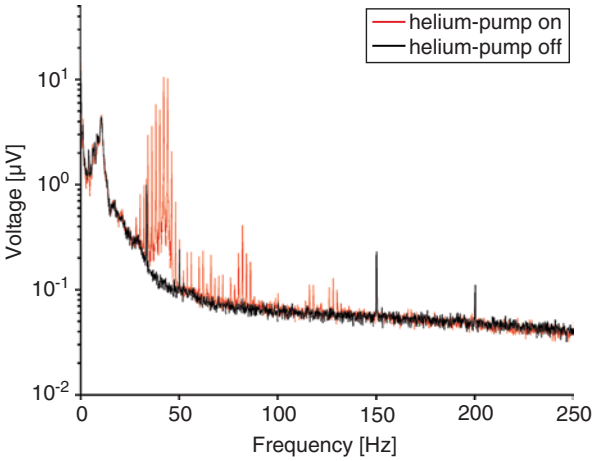

Fig. 4 Effects of the helium pump of the MR tomograph on the frequency spectrum of the EEG. These data (of 5 minutes duration for each condition) were obtained in a 1.5 Tesla Siemens Sonata scanner during non-MR-acquisition periods. Similar artefacts have been found in other MR-systems, such as the 1.5 Tesla Siemens Vision and 3 T Siemens Trio scanners. Helium-pump associated artefacts are not related to MR-image acquisition. They occur continuously, i.e. also in non-MR-acquisition periods. These artefacts are caused by the piston of the helium cooling head, which strikes the aluminium tube that functions as a cold shield. This causes vibrations of the tube at its resonance frequency of typically around 40 Hz. Vibrations of the tube induce eddy currents that generate magnetic field changes leading to the observed artefacts. The spectral peak visible in the Fourier spectrum at 50 Hz and its higher harmonics can be assigned to line noise.

to less than 5% in the study by Anami et al. (2003). Consequently, a greater dynamic range is available for the physiological EEG, allowing resolutions of 0.1 µV and below (Ritter et al. 2006; Freyer et al. 2009).

Non-MR signals such as EEG have been recorded using surplus RF receive bandwidth (Hanson et al. 2007). To this end, EEG signals amplified and digitised within the scanner are transmitted as radio waves that are detectable by the MR system and subsequently reconstructed to fill the periphery of the MRI field of view. Gradient artefacts can be greatly reduced when sampled in periods free of gradient switching using a variant of the stepping-stone technique based on a gradient field detection and gating mechanism that does not require modification of the MR sequence, in contrast to the method by Anami et al. 2003.

4.2 Synchronisation of EEG and fMRI Data Acquisitions

The EEG and fMRI acquisition systems can run independently of each other or in synchrony, with important implications for data quality (see the chapter "EEG Instrumentation and Safety" for a discussion of EEG instrumentation). While simpler to implement than synchronised acquisitions, free-running independent EEG and fMRI data acquisitions can result in a great degree of variability in the shape of the artefact (Fig. 5a and 6a), which may be more difficult to remove using post-processing methods (discussed in the next section

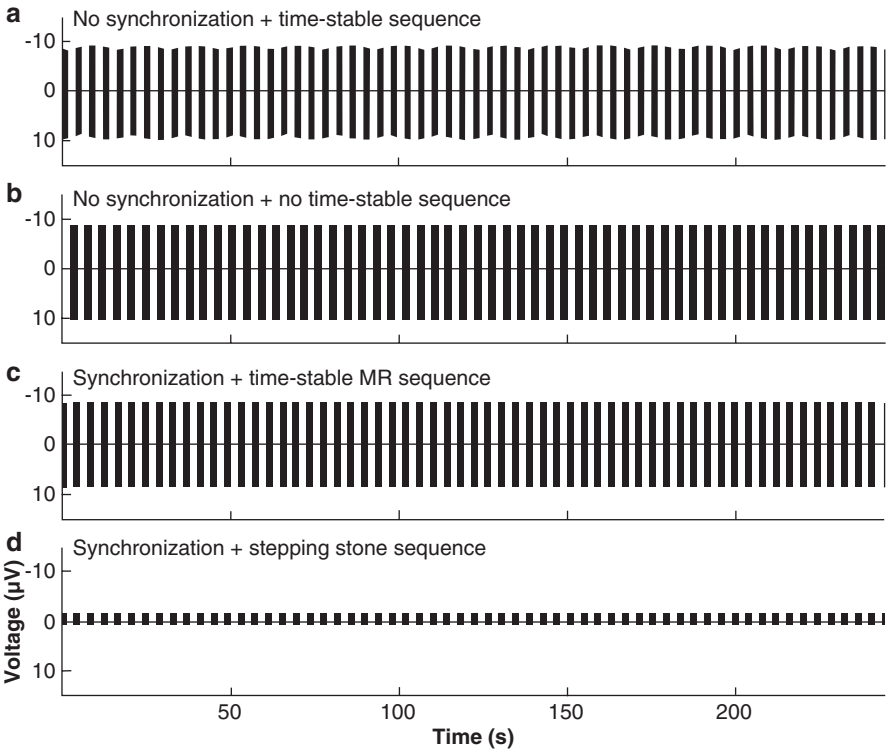

Fig. 5a–d Comparison of imaging artefact waveforms obtained from three different interleaved EEG–fMRI acquisitions: 4 min of EEG data acquired simultaneously with fMRI. Sixty MR volumes were acquired in the 4-min recording time. Due to the high amplitudes of the artefacts, physiological EEG traces in-between the image acquisition artefacts are only visible as a *flat line*. **a** Unsynchronised EEG and fMRI with a stable MR sequence and a TR that is an integer multiple of the EEG sampling rate yields EEG data containing image acquisition artefacts of high amplitudes and periodically varying shapes. **b** Unsynchronised EEG and fMRI with unstable MR sequence yields EEG data containing image acquisition artefacts of high amplitude and aperiodically varying shapes (see Fig. 5 for a zoomed-in depiction). **c** Synchronised EEG and fMRI in combination with a stable MR sequence yields image acquisition artefacts of high amplitude but constant shape (see Fig. 5). **d** Application of the *stepping-stone* sequence and synchronised EEG–fMRI yields image acquisition artefacts of lower amplitudes with constant shapes.

of this chapter). Synchronised acquisitions can be advantageous if the MR scan repetition time is chosen to be an integer multiple of the EEG sampling interval, resulting in stationary image acquisition artefacts (Fig. 5c, d and 6b), assuming that the artefact shape and amplitude do not change due to electrode movement and that the timing of the MR sequence is precise (Anami et al. 2003). In these circumstances it is possible to reduce the EEG sampling rate down to 500 Hz with satisfactory results following post-processing artefact correction (Mandelkow et al. 2006).

It should be noted that for multislice EPI sequences, the type of slice acquisition must be considered, since it influences the precision of the TR (Mandelkow et al. 2006). When slice acquisitions are equidistant in time, the actual TR can deviate from the prescribed TR by the product of the scanner clock precision and the number of slices. A stationary image acquisition artefact will be obtained if the actual TR matches a common multiple of the EEG sample time (0.2 ms for 5 kHz) and of the product of scanner clock precision (0.1 µs for 10 MHz) and number of slices. For nonequidistant slice acquisitions with pauses between successive volume acquisitions, the TR is rounded to the full precision of the scanner clock, and stationary artefacts will be obtained if TR is a multiple of the EEG sample time. Such rounding differences have been reported for the Philips 3 T Achieva system running software release 1.2.2 (Mandelkow et al. 2006) and have been found by our group for the Siemens 1.5 T Sonata system running NUMARIS/4, version syngo MR 2004A.

In a phantom measurement, Mandelkow et al. (2006) demonstrated that residual artefact power dominates the post-processed EEG spectra above roughly 80 Hz for recordings without synchronisation. This is also visible in Fig. 3a, b, which show data from a healthy subject at 1.5 T. With synchronisation, however, spectral power up to 200 Hz remains largely within 10 dB of the spectrum obtained without simultaneous fMRI (Mandelkow et al. 2006). Figure 3c, d demonstrates the superior quality of the synchronised EEG of a subject at 1.5 T.

Synchronised EEG and fMRI digitisation has been used to study high-frequency (600 Hz) and very low amplitude (few 100 nV) components of the somatosensory evoked potential (Ritter et al. 2008a ; Freyer et al. 2009) and spontaneous variations in the theta (3–6 Hz) and gamma (28–40 Hz) ranges (Giraud et al. 2007).

5 Correction of the Image Acquisition Artefact Using EEG Post-Processing

5.1 Artefact Template Subtraction

A widely applied processing method based on artefact template subtraction was demonstrated by Allen et al. (2000). This approach assumes that the shape of the gradient artefact does not change rapidly and that it is not correlated with the physiological signal (Hill et al. 1995). Channel-specific artefact templates are computed by averaging the EEG over a prespecified number of TR-related epochs and subtracted from the EEG traces in the current epoch. The epochs can be identified by recording a signal generated by the scanner that marks each image acquisition. The technique can be implemented in real time (Allen et al. 2000).

The averaging procedures implemented in different algorithms differ with respect to the number and selection of averaging epochs and their weighting. In the original implementation, the template consisted of a weighted sliding average of artefact epochs to account for possible changes of the artefact waveform over time and to account for a level of timing error, and used adaptive noise cancellation (ANC) to further reduce residual image acquisition artefacts (Allen et al. 2000). A least mean square (LMS) algorithm could be used to

adjust the weights of the ANC filter. This approach, however, needed a high sampling frequency, and some unsatisfactory results were obtained, even at sampling rates of 10 kHz (Niazy et al. 2005).

The Vision Analyzer algorithm (V.1.05.0002, BrainProducts, Munich, Germany) offers three different methods of template estimation: (1) all epochs, (2) a sliding average of a certain number of epochs, or (3) a predefined number of initial scan epochs plus subsequent epochs exceeding a predefined cross-correlation with the initial template. Instead of a specific scanner-generated signal, epochs can be identified by searching for steep gradients or high amplitudes in the EEG exceeding a defined threshold. Recently we have introduced a modified approach for dynamic template estimation where artifact epochs in the template are weighted according to a Fourier spectrum-based similarity measure. This approach allowed the recovery of ultrahigh-frequency EEG signatures with amplitudes in the nanovolt range even during image acquisition periods (Freyer et al. 2009).

Image acquisition artefact template subtraction has been successfully adopted for the reconstruction of spontaneous EEG signatures such as alpha rhythm (Goncalves et al. 2005; Laufs et al. 2003; Moosmann et al. 2003), rolandic rhythms (Ritter et al. 2008b) and epileptic activity (Benar et al. 2003; Salek-Haddadi et al. 2002, 2003) and evoked potentials in the visual (Becker et al. 2005) and somatosensory system (Schubert et al. 2008).

As noted in the previous section (on synchronisation), the quality of artefact removal by template subtraction depends on the assumption of a stationary artefact, which is best satisfied when using synchronised systems (Fig. 3c) and when the exact TR of the MR sequence is a multiple of the sampling rate of the EEG. Jitter between EEG sampling and MR acquisition results in greater residual artefacts following imaging-artefact reduction (IAR), which are particularly prominent in the frequency spectrum approximately above 50 Hz (Figs. 3c, d and 5c). Low-pass filtering (cut-off around 50 and 80 Hz) can reduce residual artefacts. Although physiological signals above the cut-off frequency are removed by this procedure too, it can still be useful for the visual evaluation of the low-frequency EEG.

An alternative to the IAR method based on the frame-by-frame identification of the artefact uses an adaptive finite impulse response (FIR) filter (Wan et al. 2006). This method also assumes that the image acquisition artefacts are temporally stationary, except for a small frame-by-frame time shift. Using a Taylor expansion based on the average artefact waveform, the time-shifted image acquisition artefact of each frame was estimated using the average artefact waveform and its derivatives by LMS fitting. The algorithm outperformed simple average artefact template subtraction, which equals a zeroth-order FIR filter, but was not compared to artefact template subtraction combined with timing error correction.

An alternative to average artefact template subtraction, but one that is closely related to it, is based on online subtraction of a model of the image acquisition artefact that is estimated prior to EEG recording and subsequently fitted to the ongoing EEG for subtraction (Garreffa et al. 2003). A commercial software solution is also available for real-time imaging-artefact correction based on gradient template subtraction and template drift compensation (TDC) (Vision RecView, MRI correction module, Brainproducts, Munich, Germany). In this case, synchronised EEG–fMRI is highly beneficial.

5.2 Computing and Correcting Timing Errors

Since image acquisition artefacts contain higher frequencies than the EEG sampling rate, timing errors can lead to considerable changes of the image acquisition artefact waveform in unsynchronised acquisitions. Therefore, timing errors must be considered in the calculation of the average artefact template and in subsequent template subtraction to achieve adequate artefact reduction.

One method is to divide data into epochs, each containing an MRI volume or scan acquisition period. The epochs are then interpolated (usually by a sinc function with a factor of 10–15) and subsequently aligned by maximising the cross-correlation to a reference period. After adjusting, epochs are downsampled to the original sampling frequency and subsequently averaged to calculate an artefact template (Allen et al. 2000; Negishi et al. 2004).

Another method relies on the calculation of multiple image acquisition artefact templates, each representing another waveform of the artefact (Benar et al. 2003). This algorithm is implemented in Vision Analyzer (V.1.05.0004), providing so-called template drift detection (TDD) and subsequent TDC. Using the drift information provided by TDD, different average-artefact templates are calculated. Each individual artefact is assigned to one template. Artefact correction is then obtained by subtracting the corresponding template from the respective artefact epoch.

Figure 5 shows two cases of unsynchronised EEG–fMRI acquisitions that require different strategies for optimal artefact correction. Figure 5a shows an EEG recorded during fMRI with a temporally stable sequence and with a TR that is an integer multiple of the EEG sampling time. In this case of periodically changing artefact waveforms, an efficient correction would be to bin the observed types of artefact waveforms and then perform selective template calculation and subtraction. Interpolation of artefact periods would not eliminate the systematic differences between successive periods. Figure 5b depicts unsynchronised EEG acquisition during an fMRI sequence that was neither temporally stable nor an integer multiple of the EEG sampling interval. This case would benefit from the interpolation of artefact epochs rather than from binning, due to the large inter-artefact waveform variability.

5.3 Temporal Principal Component Analysis

Violations of the stationarity assumption can occur independent of the degree of EEG and fMRI acquisition due to electrode movement in relation to the gradient coil and RF antenna, leading to a degradation in artefact template subtraction performance.

Negishi and colleagues proposed the application of temporal principal component analysis (PCA) to each EEG channel independently in order to remove residual artefacts (Negishi et al. 2004). Temporal PCA utilises the differential statistical characteristics of the variance of EEG epochs during and in-between scan acquisitions, yielding results similar to those obtained using IAR + ANC (Negishi et al. 2004).

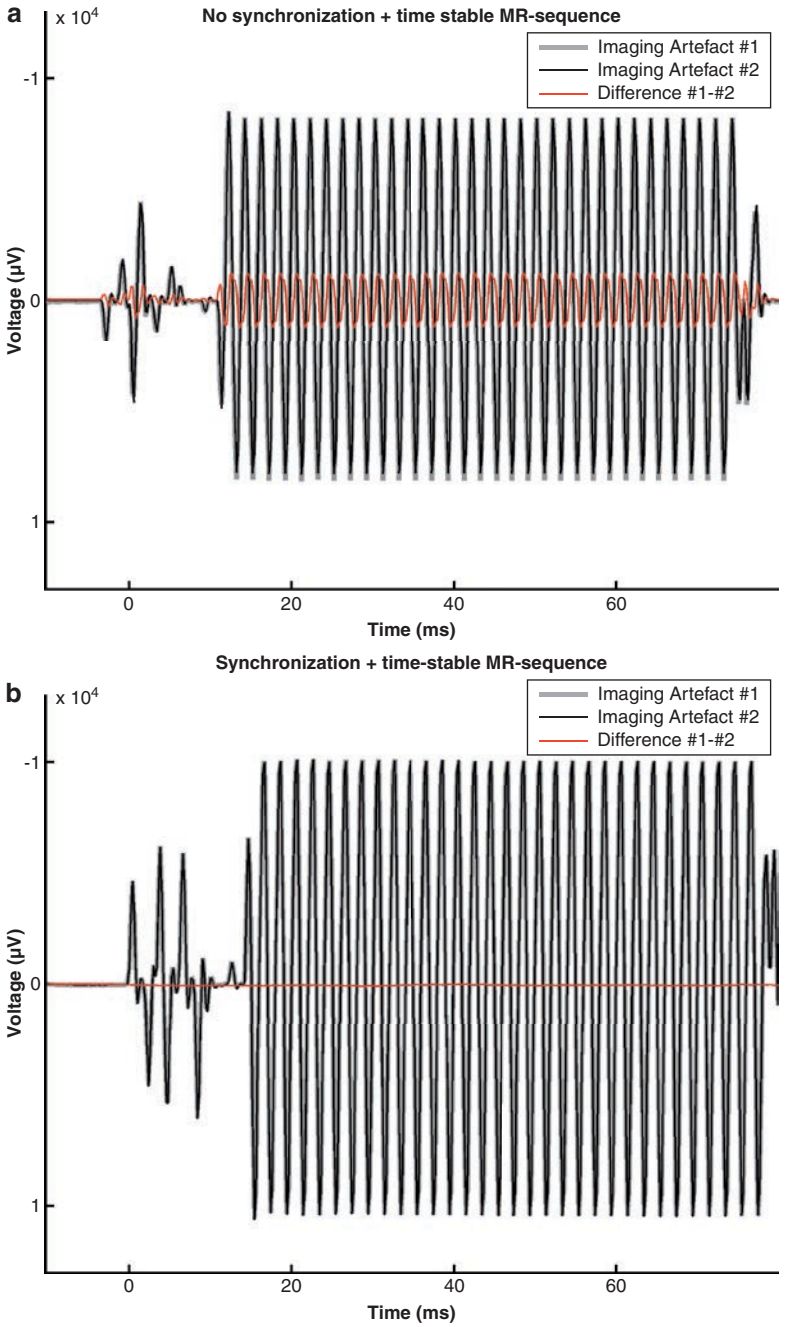

Fig. 6a–b Stability of image acquisition artefacts: single-slice artefacts of two consecutive imaging volume artefacts are superimposed for comparison (black and grey line). Red indicates the difference wave for the two artefacts. **a** In the unsynchronised EEG–fMRI approach, consecutive image acquisition artefacts differ considerably, resulting in a distinct difference wave. **b** In the synchronised EEG–fMRI approach, consecutive image acquisition artefacts are identical, resulting in a difference wave that is almost zero and zero (i.e. only the physiological EEG signal is present).

The method called fMRI artefact slice template removal (FASTR) employs both artefact template subtraction and temporal PCA (Niazy et al. 2005). Again, slice-specific artefact templates are constructed as the local moving average plus a linear combination of basis functions describing the variation of residuals. The basis functions are derived by performing temporal PCA on the artefact residuals and selecting the dominant components to serve as a basis set. Finally, imaging artefact residuals are removed by an ANC filter (see below). This algorithm has been successfully applied in a continuous EEG–fMRI study of laser-evoked responses at 3 T (Iannetti et al. 2005) When the EEG signature of interest is of very high frequency, the beneficial outcome of a PCA-based postprocessing can be further enhanced by employing a band-specific PCA in the high-frequency band in addition to the PCA on the broad-band EEG. This cascaded PCA postprocessing enables the recovery of ultrafast EEG signatures, which were otherwise obscured by imaging artifact residuals (Freyer et al. 2009).

5.4 Independent Component Analysis

Another approach to imaging artefact correction is independent component analysis (ICA) in addition to artefact template subtraction (Mantini et al. 2007). ICA is a signal processing technique that recovers independent sources from a set of simultaneously recorded signals that result from a linear mixing of the source signals (Hyvarinen 1999; Mantini et al. 2007). Since EEG and image acquisition artefacts are generated by different independent processes and are therefore uncorrelated, ICA seems to be an appropriate approach. Mantini and colleagues categorised the ICA sources into two signal categories: brain signals and artefacts. This was done by visual inspection or in an automated approach by correlation to reference signals. Only sources classified as nonartificial were back-projected and used for further analysis. This approach proved to be capable of not only removing residual image acquisition artefacts but also ballistocardiogram and ocular artefacts.

Grouiller et al. (2007) compared an ICA-based imaging artefact removal approach to three other fundamental approaches to imaging artefact correction: IAR (Allen et al. 2000), FMRIB (Niazy et al. 2005) and Fourier transform (FT) filtering (Hoffmann et al. 2000). They used the implementation of the Infomax ICA algorithm in the EEGLAB toolbox (Computational Neurobiology Laboratory, Salk Institute, La Jolla, CA, USA: http://www.sccn.ucsd.edu/eeglab/) (Bell and Sejnowski 1995). The authors selected the components that were correlated with the imaging artefact template. Selected components had a normalised cross-correlation coefficient higher than the average plus one standard deviation of that coefficient computed for all the components. The components representing image acquisition artefacts were excluded from the EEG reconstruction. Results for the performance of ICA, however, differed between simulations and real data (for details, see Sect. 6). Results obtained by Grouiller et al. (2007) indicate that ICA may not be applicable for efficiently estimating independent components in long time series of EEG data. A theoretical reason for this may be the spatial nonstationarity of the EEG and (especially) of the imaging artefact signal.

5.5 Filtering in the Frequency Domain

Image acquisition artefacts are periodic and distributed over a limited range of frequencies, suggesting that correction may be performed satisfactorily on the frequency domain. One such method is based on the comparison of the spectral content of EEG data acquired with and without simultaneous MR acquisition. The Fourier components of the signal corresponding to the MR-specific frequencies are set to zero for subsequent reprojection in signal space (Hoffmann et al. 2000). This algorithm was implemented in the FEMR program provided by Schwarzer (Munich, Germany). The disadvantage of this method is that, due to a spectral overlap between the physiological EEG and image acquisition artefacts, some of the physiological EEG signal is removed as well. The method is characterised by ringing artefact (Benar et al. 2003), which results from discontinuities (e.g. gaps between scan acquisitions in interleaved EEG–fMRI) in the signals to be corrected. A similar approach relies on channel-wise subtraction of an average gradient artefact power spectrum—adapted by a scaling factor to the spectrum of the individual artefact—from the power spectrum of the artefact-distorted EEG (Sijbers et al. 1999). To filter image acquisition artefacts in the frequency domain, one group (Grouiller et al. 2007) first calculated the FT of the imaging artefact template. Then, weights were applied to the spectral components of the FT of the EEG. For spectral components of the artefact afflicted EEG corresponding to strong spectral components in the artefact template, spectral filtering weights were set to the inverse. Thus, coefficients corresponding to the image acquisition artefact were attenuated. To obtain the corrected EEG, the inverse FT was applied. Grouiller et al. (2007) reported weighting coefficients to be inversely proportional to FT coefficients of the artefacts instead of zeroing them (Hoffmann et al. 2000) improved signal preservation and reduced ringing.

6 Evaluation of Correction Methods

To date, artefact correction performance evaluation has not been performed consistently. In many EEG–fMRI studies, a single algorithm is chosen without proper justification, and often the quality of gradient artefact correction is assessed by visual inspection only. However, a more systematic approach to the choice of correction method may be advised for certain applications, such as the analysis of single events and nonaveraged EEG data, when residual artefacts do not cancel out, or those that rely on the quantitation of EEG power in certain spectral bands. The task of selecting a suitable correction algorithm would be greatly facilitated by standardising their evaluation and carefully considering the experimental requirements in terms of the EEG–fMRI protocol and features of the signal of interest (spectral signature, amplitude). In the following we describe the main evaluation strategies employed to date.

Knowledge of the true signal is highly advantageous for the evaluation of signal filtering methods. This can be obtained in tests on phantoms and using signals generated by

instruments offering the opportunity to assess both signal preservation and artefact reduction (Negishi et al. 2004; Schmid et al. 2006). Simulations have also been employed in which artificially generated signals (e.g. those extracted from recordings made under the control condition or simulated mathematically) are added to true artefacts (Allen et al. 2000; Groullier et al. 2007). The main disadvantage of this approach is a lack of realism, in terms of the complexity of true physiological signals, noise, subject movement and intersubject and inter-recording variability.

For tests based on real EEG, EEG recorded outside the MR environment should constitute the best gold standard. However, the specific evaluation of image acquisition artefact reduction methods can be performed adequately from signals recorded inside the scanner to compare signals captured without scanning (reference) and with scanning (and correction). For example, Allen et al. compared the signal's spectral content using this approach (Allen et al. 2000). In theory, a drawback of this approach is a lack of knowledge of the true EEG signal, in part due to the additional effects of the pulse artefact but also the sequential nature of the samples used for comparison. On the other hand, image acquisition artefact correction method performance evaluations based on signals recorded exclusively inside the scanner have the advantage that the pulse artefact is a common factor. Nonetheless, sequential measurements under the two experimental conditions may be particularly problematic for signals of interest with a high intrinsic variability, such as brain rhythms or epileptic discharges, but are possibly less so for evoked responses, where reproducible neuronal signals are more likely, although this bias can be reduced through adequate sampling.

Benar et al. (2003) compared Fourier filtering and template subtraction using EEGs obtained from patients with epilepsy, which were inspected by a trained observer after the application of both artefact correction methods. Visual subtraction was found to result in higher EEG quality than Fourier filtering.

Different gradient artefact correction algorithms based on the approach of template artefact subtraction were evaluated on data recorded with an unsynchronised EEG–fMRI setup using a visual stimulus presented to subjects at rest (Ritter et al. 2007). In this study, a combination of the following analyses was employed for performance estimation: (1) the degree of artefact reduction was evaluated by comparing the spectral content of the corrected data to that of gradient artefact free EEG epochs for six predefined frequency bands ranging from theta to omega (1–250 Hz); (2) the preservation of non-gradient artefact components of the EEG after correction was evaluated twofold—by comparing the spectral content of non-acquisition EEG epochs before and after gradient artefact correction for the six predefined frequency bands, and by exploring the impact of artefact correction on artificially generated signals added to the EEG. The study demonstrated that the amount of artefact reduction and the degree of physiological signal preservation are important complementary performance measures.

Another approach to the comparison of different artefact correction algorithms was based on the generation of artificial EEG and artificial image acquisition artefacts by a simple forward model (Grouiller et al. 2007). Modulations of the imaging artefact amplitude caused by subject motion and MRI and EEG clock asynchrony—which are typical of unsynchronised EEG-MRI setups—in combination with different EEG sampling rates were implemented in the model. The advantages of this approach include: it allows the effects of

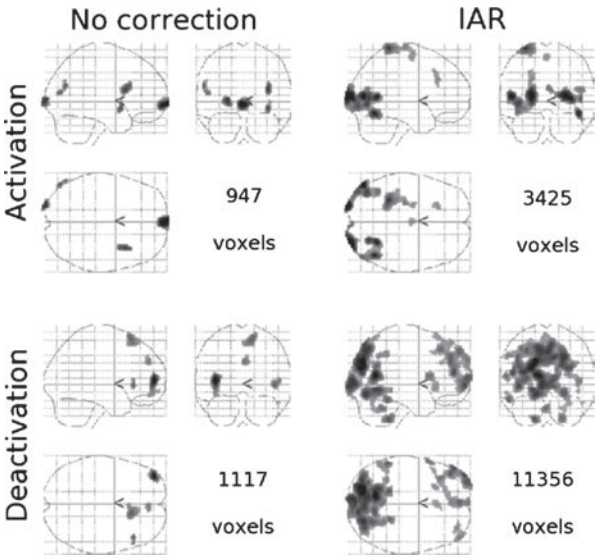

Fig. 7 Dependence of FMRI correlates of the alpha rhythm on the quality of image acquisition artefact correction. Glass brains were obtained using the power in the alpha band as a regressor convolved with the HRF (p = 0.005, uncorrected). Left: Without any artefact correction. Right: Using IAR image acquisition artefact removal. (Modified from Grouiller et al. 2007).

different experimental or empirical parameters to be tested; knowledge of ground truth. The same group also evaluated artefact correction in real EEG data. To this end, after artefact correction, they calculated correlation coefficients between the alpha power modulated by an eyes-open/eyes-closed paradigm and the task function and also correlation coefficients between interictal spikes acquired inside and outside the scanner. For the simulated data, the authors found that the ICA algorithm was the method that presented by far the best average results, although with a high performance variability, indicating that this approach might be unstable. FASTR and IAR were approximately equivalent and FT performed significantly less well. For the real data, the IAR and FASTR algorithms obtained the best results. There was considerable discrepancy between the results obtained from simulations and from experimental data for the ICA approach, indicating a possible weakness of the modelling.

The authors assessed the effect of artefact correction on the fMRI results by comparing statistical parametric maps obtained from models based on alpha power with and without imaging artefact correction (Fig. 7). ”Summarized, the discussed repertoire of available hardware and software solutions enables satisfying imaging-artefact correction. However, individual results can vary and therefore a continuous critical re-evaluation of results is necessary to ensure reasonable data quality.”

Acknowledgements We would like to thank Daniel Margulies and Matthias Reinacher for proofreading the manuscript. This work was supported by the German Federal Ministry of Education and Research BMBF (Berlin Neuroimaging Center; Bernstein Center for Computational Neuroscience) and the German Research Foundation DFG (Berlin School of Mind and Brain.

References

Allen PJ, Josephs O, Turner R (2000) A method for removing imaging artifact from continuous EEG recorded during functional MRI. Neuroimage 12(2):230–239

Anami K, Mori T, Tanaka F, Kawagoe Y, Okamoto J, Yarita M, Ohnishi T, Yumoto M, Matsuda H, Saitoh O (2003) Stepping stone sampling for retrieving artifact-free electroencephalogram during functional magnetic resonance imaging. Neuroimage 19(2 Pt 1):281–295

Baudewig J, Bittermann HJ, Paulus W, Frahm J (2001) Simultaneous EEG and functional MRI of epileptic activity: a case report. Clin Neurophysiol, 112: 1196–200

Becker R, Ritter P, Moosmann M, Villringer A (2005) Visual evoked potentials recovered from fMRI scan periods. Hum Brain Mapp 26(3):221–230

Bell AJ, Sejnowski TJ (1995) An information-maximization approach to blind separation and blind deconvolution. Neural Comput 7(6):1129–1159

Benar C, Aghakhani Y, Wang Y, Izenberg A, Al Asmi A, Dubeau F, Gotman J (2003) Quality of EEG in simultaneous EEG–fMRI for epilepsy. Clin Neurophysiol 114(3):569–580

Felblinger J, Slotboom J, Kreis R, Jung B, Boesch C (1999) Restoration of electrophysiological signals distorted by inductive effects of magnetic field gradients during MR sequences. Magn Reson Med 41(4):715–721

Freyer F, Becker R, Anami K, Curio G, Villringer A, Ritter P. Ultrahigh-frequency EEG during fMRI: Pushing the limits of imaging-artifact correction. Neuroimage, 2009

Garreffa G, Carni M, Gualniera G, Ricci GB, Bozzao L, De Carli D, Morasso P, Pantano P, Colonnese C, Roma V, et al. (2003) Real-time MR artifacts filtering during continuous EEG/fMRI acquisition. Magn Reson Imaging 21(10):1175–1189

Giraud AL, Kleinschmidt A, Poeppel D, Lund TE, Frackowiak RS, Laufs H (2007) Endogenous cortical rhythms determine cerebral specialization for speech perception and production. Neuron 56(6):1127–1134

Goldman RI, Stern JM, Engel J Jr., Cohen MS (2000) Acquiring simultaneous EEG and functional MRI. Clin Neurophysiol 111(11):1974–1980

Goldman RI, Stern JM, Engel J, Jr., Cohen MS (2002) Simultaneous EEG and fMRI of the alpha rhythm. Neuroreport, 13: 2487–92

Goncalves SI, de Munck JC, Pouwels PJ, Schoonhoven R, Kuijer JP, Maurits NM, Hoogduin JM, Van Someren EJ, Heethaar RM, Lopes da Silva FH. (2005) Correlating the alpha rhythm to BOLD using simultaneous EEG/fMRI: Inter-subject variability. Neuroimage

Grouiller F, Vercueil L, Krainik A, Segebarth C, Kahane P, David O (2007) A comparative study of different artefactartefact removal algorithms for EEG signals acquired during functional MRI. Neuroimage 38(1):124–137

Hanson LG, Lund TE, Hanson CG (2007) Encoding of electrophysiology and other signals in MR images. J Magn Reson Imaging 25(5):1059–1066

Hill RA, Chiappa KH, Huang-Hellinger F, Jenkins BG (1995) EEG during MR imaging: differentiation of movement artifact from paroxysmal cortical activity. Neurology, 45: 1942–3

Hoffmann A, Jager L, Werhahn KJ, Jaschke M, Noachtar S, Reiser M (2000) Electroencephalography during functional echo-planar imagingecho-planar imaging: detection of epileptic spikes using post-processing methods. Magn Reson Med 44(5):791–798

Horovitz SG, Rossion B, Skudlarski P, Gore JC (2004) Parametric design and correlational analyses help integrating fMRI and electrophysiological data during face processing. Neuroimage., 22: 1587–95

Horovitz SG, Skudlarski P, Gore JC (2002) Correlations and dissociations between BOLD signal and P300 amplitude in an auditory oddball task: a parametric approach to combining fMRI and ERP. Magn Reson.Imaging, 20: 319–25

Huang-Hellinger FR, Breiter HC, McCormack GM, Cohen MS, Kwong KK, Savoy RL, Weisskoff RM, Davis TL, Baker JR, Belliveau JW, et al. (1995) Simultaneous functional magnetic resonance imaging and electrophysiological recording. Human Brain Mapp 3:13–23

Hyvarinen A (1999) Fast and robust fixed-point algorithms for independent component analysis. IEEE Trans Neural Netw, 10: 626–34

Iannetti GD, Niazy RK, Wise RG, Jezzard P, Brooks JC, Zambreanu L, Vennart W, Matthews PM, Tracey I (2005) Simultaneous recording of laser-evoked brain potentials and continuous, high-field functional magnetic resonance imaging in humans. Neuroimage 28(3):708–719

Ives JR, Warach S, Schmitt F, Edelman RR, Schomer DL (1993) Monitoring the patient's EEG during echo planar MRI. Electroencephalogr. Clin. Neurophysiol 87: 417–20

Krakow K, Woermann FG, Symms MR, Allen PJ, Lemieux L, Barker GJ, Duncan JS, Fish DR (1999) EEG-triggered functional MRI of interictal epileptiform activity in patients with partial seizures. Brain, 122: 1679–88

Kruggel F, Wiggins CJ, Herrmann CS, von Cramon DY (2000) Recording of the event-related potentials during functional MRI at 3.0 Tesla field strength. Magn Reson.Med., 44: 277–82

Laufs H, Kleinschmidt A, Beyerle A, Eger E, Salek-Haddadi A, Preibisch C, Krakow K (2003) EEG-correlated fMRI of human alpha activity. Neuroimage., 19: 1463–76

Lemieux L, Allen PJ, Franconi F, Symms MR, Fish DR (1997) Recording of EEG during fMRI experiments: patient safety. Magn Reson Med 38(6):943–952

Lemieux L, Krakow K, Fish DR (2001) Comparison of spike-triggered functional MRI BOLD activation and EEG dipole model localization. Neuroimage 14: 1097–104

Mandelkow H, Halder P, Boesiger P, Brandeis D (2006) Synchronization facilitates removal of MRI artefacts from concurrent EEG recordings and increases usable bandwidth. Neuroimage 32(3):1120–1126

Mantini D, Perrucci MG, Cugini S, Ferretti A, Romani GL, Del Gratta C (2007) Complete artifact removal for EEG recorded during continuous fMRI using independent component analysis. Neuroimage 34(2):598–607

Moosmann M, Ritter P, Krastel I, Brink A, Thees S, Blankenburg F, Taskin B, Obrig H, Villringer A (2003) Correlates of alpha rhythm in functional magnetic resonance imaging and near infrared spectroscopy. Neuroimage, 20: 145–58

Negishi M, Abildgaard M, Nixon T, Constable RT (2004) Removal of time-varying gradient artifacts from EEG data acquired during continuous fMRI. Clin Neurophysiol 115(9): 2181–2192

Niazy RK, Beckmann CF, Iannetti GD, Brady JM, Smith SM (2005) Removal of FMRI environment artifacts from EEG data using optimal basis sets. Neuroimage 28(3):720–737

Opitz B, Mecklinger A, Von Cramon DY, Kruggel F (1999) Combining electrophysiological and hemodynamic measures of the auditory oddball. Psychophysiology, 36: 142–7

Ritter P, Becker R, Graefe C, Villringer A (2007) Evaluating gradientgradient artifact correction of EEG data acquired simultaneously with fMRI. Magn Reson Imaging 25(6):923–932

Ritter P, Freyer F, Becker R, Anami K, Curio G, Villringer A (2006) Recording of ultrafast (600 Hz) EEG oscillations with amplitudes in the nanovolt range during fMRI-acquisition periods. 14th Scientific Meeting ISMRM, Seattle, WA, USA, 6–12 May 2006

Ritter P, Freyer F, Curio G, Villringer A (2008a) High frequency (600 Hz) population spikes in human EEG delineate thalamic and cortical fMRI activation sites. Neuroimage 42(2): 483–490

Ritter P, Moosmann M, Villringer A (2008b) Rolandic alpha and beta EEG rhythms' strengths are inversely related to fMRI-BOLD signal in primary somatosensory and motor cortex. Hum Brain Mapp 30(4):1168–1187

Salek-Haddadi A, Lemieux L, Merschhemke M, Friston KJ, Duncan JS, Fish DR (2003) Functional magnetic resonance imaging of human absence seizures. Ann.Neurol, 53: 663-7

Salek-Haddadi A, Merschhemke M, Lemieux L, Fish DR (2002) Simultaneous EEG-Correlated Ictal fMRI. Neuroimage, 16: 32–40

Schmid MC, Oeltermann A, Juchem C, Logothetis NK, Smirnakis SM (2006) Simultaneous EEG and fMRI in the macaque monkey at 4.7 Tesla. Magn Reson.Imaging., 24: 335–42

Schubert R, Ritter P, Wustenberg T, Preuschhof C, Curio G, Sommer W, Villringer A (2008) Spatial attention related SEP amplitude modulations covary with BOLD signal in S1–a simultaneous EEG–fMRI study. Cereb Cortex, 18: 2686–700

Seeck M, Lazeyras F, Michel CM, Blanke O, Gericke CA, Ives J, Delavelle J, Golay X, Haenggeli CA, de Tribolet N, Landis T (1998) Non-invasive epileptic focus localization using EEG-triggered functional MRI and electromagnetic tomography. Electroencephalogr.Clin. Neurophysiol 106: 508–12

Sijbers J, Michiels I, Verhoye M, Van Audekerke J, Van der LA, Van Dyck D (1999) Restoration of MR-induced artifacts in simultaneously recorded MR/EEG data. Magn Reson Imaging 17(9):1383–1391

Symms MR, Allen PJ, Woermann FG, Polizzi G, Krakow K, Barker GJ, Fish DR, Duncan JS (1999) Reproducible localization of interictal epileptiform discharges using EEG-triggered fMRI. Phys.Med.Biol., 44: N161–N8

Sommer M, Meinhardt J, Volz HP (2003) Combined measurement of event-related potentials (ERPs) and fMRI. Acta Neurobiol.Exp.(Wars.), 63: 49–53

Van Audekerkea J, Peeters R, Verhoye M, Sijbers J, Van der LA (2000) Special designed RF-antenna with integrated non-invasive carbon electrodes for simultaneous magnetic resonance imaging and electroencephalography acquisition at 7T. Magn Reson Imaging 18(7):887–891

Warach S, Ives JR, Schlaug G, Patel MR, Darby DG, Thangaraj V, Edelman RR, Schomer DL (1996) EEG-triggered echo-planar functional MRI in epilepsy. Neurology, 47: 89–93

Wan X, Iwata K, Riera J, Kitamura M, Kawashima R (2006) Artifact reduction for simultaneous EEG/fMRI recording: adaptive FIR reduction of imaging artifacts. Clin Neurophysiol 117(3):681–692